Chinese Chemical Letters 35 (2024) 108637

Contents lists available at ScienceDirect

Chinese Chemical Letters

journal homepage: www.elsevier.com/locate/cclet

Preparation and performance of novel magnetic phase-change-microcapsule-supported Bi_2WO_6 catalyst

Zhuoni Jiang[a,b], Zhiqing Ge[a], Shuo Yan[a], Jingjing Shu[a], Mozhen Wang[a,*], Xuewu Ge[a,*]

[a] Key Laboratory of Precision and Intelligent Chemistry, Department of Polymer Science and Engineering, University of Science and Technology of China, Hefei 230026, China
[b] School of Materials Science and Engineering, Southwest University of Science and Technology, Mianyang 621010, China

ARTICLE INFO

Article history:
Received 9 May 2022
Revised 29 May 2023
Accepted 31 May 2023
Available online 3 June 2023

Keywords:
Photocatalyst
Phase change microcapsules
Self-temperature regulation
Bismuth tungstate
Magnetic separation

ABSTRACT

The design and synthesis of novel photocatalyst with self-temperature control function is an important topic in the field of advanced environmental functional materials. In this work, submicron-sized magnetic phase change microcapsules composed of paraffin core and Fe_3O_4-loaded silica shell are prepared, on which the Bi_2WO_6 crystals is grown *in situ* through hydrothermal reaction to obtain novel magnetic phase-change-microcapsule-supported Bi_2WO_6 catalyst (MP@FS/BWO). The MP@FS/BWO has a paraffin encapsulation ratio of 57.1%, and the phase change enthalpy of 105.1 J/g in a temperature range of 50–60 °C, which endows the MP@FS/BWO with a certain self-temperature regulation ability. MP@FS/BWO shows excellent catalytic performance in the decomposition of rhodamine B under the simulated sunlight irradiation. After the light source is turned off, it still has good catalytic ability by maintaining high temperature due to its temperature control function based on the phase transition process. The MP@FS/BWO can be easily recycled by magnetic separation and shows good structural stability and reusability. This work provides a new idea for the development of long-effect and energy-saving outdoor photocatalysts.

Bismuth tungstate is a semiconductor material with a narrow band gap (~2.7 eV) and shows high photocatalytic activity in the decomposition of organic pollutants under visible light [1–8]. It has been found that the photocatalytic performance of Bi_2WO_6 are closely related to its particle morphology, which includes nanospheres, flower petal, nanosheets, and so on [9–12]. In addition, the smaller the size of Bi_2WO_6, the higher the photocatalytic efficiency [9]. The nanosheet-like Bi_2WO_6 has a narrower band gap and a higher surface area compared to the others, resulting in a better light absorption and photocatalytic performance than the others [10]. However, the reusability of nano-sized Bi_2WO_6 is limited by the difficulty in the separation and recycle of nanoparticles with traditional separation methods, such as centrifugation and precipitation. Magnetic separation is a simple and effective method to recycle the nanoparticles [13,14]. For example, Zhang *et al.* [15] loaded Bi_2WO_6 nanoparticles (5–15 nm) on Fe_3O_4 nanoparticles to obtain a core-shell structure Fe_3O_4@Bi_2WO_6 particles with a size of 300–400 nm, which can be separated from aqueous solution in dozens of seconds using a magnet. The catalytic performance of the recycled Fe_3O_4@Bi_2WO_6 nanoparticles on the decomposition of methylene blue (MB) under visible light was barely changed after five cycles.

On the other hand, the efficiency of photocatalysts also depends on the temperature of the reaction system [16–19]. Ishiki *et al.* [19] studied the decomposition of imazethapyr in an aqueous suspension of TiO_2 nanoparticles at the temperature ranging from 20 °C to 40 °C under solar radiation, and found that the decomposition rate of imazethapyr is faster at 20 °C than that at 40 °C. However, the temperature of the catalytic system cannot be self-controlled at a relatively low temperature under the irradiation of sunlight. Therefore, the design and preparation of photocatalyst with self-temperature control function is a worthwhile research topic.

It is well-known that solid-liquid phase change materials are widely used to self-regulate temperature due to its ability to store/release thermal energy during reversible phase-change processes [20–23]. Currently, some complexes of photocatalysts and phase change materials have been reported [24–27]. For example, Chai *et al.* [27] synthesized spherical microcapsules (n-eicosane@TiO_2) having n-eicosane core with a mass fraction of 65.5% and a smooth TiO_2 shell. The decomposition of n-eicosane@TiO_2 microsphere to MB reaches 90% under the UV irradiation. In addition to good photocatalytic effect for the chemical decomposition, n-eicosane@TiO_2 microsphere also have high

* Corresponding authors.
E-mail addresses: pstwmz@ustc.edu.cn (M. Wang), xwge@ustc.edu.cn (X. Ge).

https://doi.org/10.1016/j.cclet.2023.108637
1001-8417/

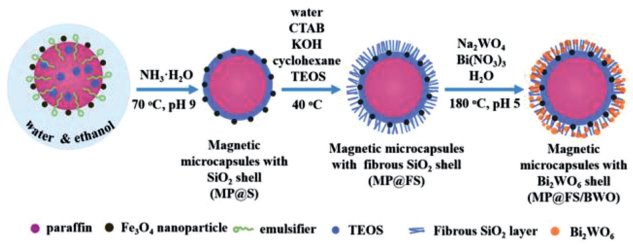

Scheme 1. Preparation process of magnetic phase-change-microcapsule-supported Bi_2WO_6 catalyst.

encapsulation efficiency (65.6%) and high thermal-storage capability. However, the interaction between phase change behavior and photocatalytic properties has not been discussed and deserves further study.

In this paper, novel magnetic phase-change-microcapsule-supported Bi_2WO_6 catalyst (MP@FS/BWO) are fabricated, as shown in Scheme 1. First, an emulsion was prepared using an aqueous dispersion of Fe_3O_4 nanoparticles (NPs) with an average diameter of about 6 nm (Fig. S1 in Supporting information) and the emulsifier cetyl trimethyl ammonium bromide (CTAB) as the water phase and a mixture of paraffin and tetraethyl orthosilicate (TEOS) as the oil phase. Then, the hydrolysis and condensation reaction of TEOS is catalyzed at the interface of the paraffin emulsion droplets by the addition of $NH_3·H_2O$ to form primary magnetic phase change microcapsules (MP@S), which are composed of a paraffin core and a solid silica shell decorated with Fe_3O_4 NPs, as shown in Fig. 1a. The diameter of spherical MP@S microcapsules ranges from 120 nm to 500 nm. The FTIR spectrum of MP@S is shown in Fig. 1b, compared with those of paraffin and Fe_3O_4. The deformation vibration peaks of the methylene group of long-chain alkanes (722 cm^{-1}), the stretching vibration of Fe–O–Fe (592 cm^{-1}), and the asymmetric (2963 cm^{-1}, 2920 cm^{-1}) and symmetric (2869 cm^{-1}, 2843 cm^{-1}) stretching vibration peaks of C–H in $-CH_3$ and $-CH_2-$ groups can be clearly distinguished on the IR spectrum of MP@S. The absorption at 1053 cm^{-1} and 800 cm^{-1} could be assigned to the asymmetric stretching vibration of Si–O–Si and the symmetric stretching vibration of Si–O. The above results indicate MP@S is composed of paraffin, Fe_3O_4 and SiO_2. The encapsulation ratio of paraffin (Er) defined as the mass fraction of paraffin in the microcapsules can be quantitatively measured by thermogravimetric analysis (TGA) [28]. As shown in Fig. 1c, the weight loss between 150 °C and 320 °C on the TG curve of MP@S should be caused by the decomposition of paraffin. Therefore, the Er of MP@S can be calculated to be 80.8%. The residual mass above 400 °C should be assigned to the total mass of Fe_3O_4 and silica shell for MP@S.

Next, a layer of fibrous silica (F-SiO_2) is grown on the outer surface of the MP@S microcapsules according to our previous work [15,29-33] to obtain MP@FS microcapsules. The thickness of the F-SiO_2 layer is about 30 nm, as presented in Fig. 1d. The N_2 adsorption-desorption isotherms and the corresponding pore size distributions of MP@FS (Fig. S2a in Supporting information) show that MP@FS has a mesoporous structure with a most probable pore size of about 15 nm. The BET surface area is accordingly calculated to be as high as 213.8 m^2/g.

Finally, the precursors of Bi_2WO_6, *i.e.*, WO_4^{2-} and Bi^{3+} ions, are adsorbed on the F-SiO_2 layer and hydrolyze *in situ* to form a shell composed of Bi_2WO_6 nanoparticles at 180 °C and pH 5, forming the product MP@FS/BWO microcapsules with a particle diameter of 500–800 nm, as shown in Fig. 1e. The primary solid silica shell of MP@S will not be etched at the current reaction condition [15], which protects the coated paraffin from leakage. The FTIR spectrum of MP@FS/BWO can be seen in Fig. 1b. In addition to the characteristic absorption peaks of paraffin, SiO_2 and Fe_3O_4 contained in MP@S, there is also a W-O stretching vibration peak at 726 cm^{-1}. The distribution of Bi and W elements of MP@FS/BWO was confirmed by the EDS mapping images in Fig. 1f, which presents that Si, Bi, and W elements are uniformly distributed around the microcapsules. XRD diagram of MP@FS/BWO in Fig. 1g shows the diffraction peaks (21.5° and 23.8°) of paraffin (JCPDS Card No. 40–1995), the diffraction peaks (30.3° and 35.7°) of Fe_3O_4 (JCPDS Card No. 19–0629), and the diffraction peaks (28.5°, 33.0°, 56.0° and 58.3°) of Bi_2WO_6 (JCPDS Card No. 26–1044). The above results indicate the presence of paraffin, SiO_2, Fe_3O_4, and Bi_2WO_6 in MP@FS/BWO. The TEM image of MP@FS/BWO in Fig. 1e clearly shows the stack of Bi_2WO_6 nanosheets on the surface of the particles. It is noted that the core-shell structure of MP@FS/BWO cannot be observed from the inset of Fig. 1e. The reason is that Bi and W elements with high atomic numbers adsorbed on the F-SiO_2 shell have strong electron scattering ability, making it difficult for electrons to penetrate the sample. The Er

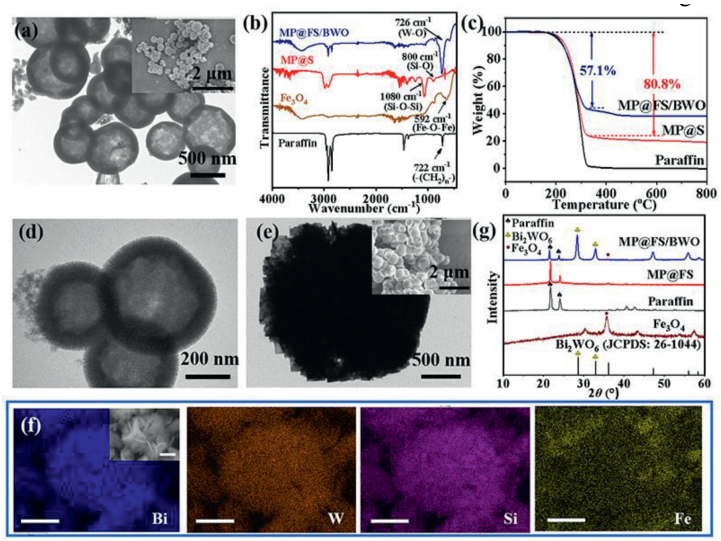

Fig. 1. (a) TEM image of MP@S, the inset is the corresponding SEM image. (b) FTIR spectra of paraffin, Fe_3O_4, MP@S, and MP@FS/BWO. (c) TG curves of paraffin, MP@S, and MP@FS/BWO. (d) TEM image of MP@FS. (e) TEM image of MP@FS/BWO, the inset is the corresponding SEM image. (f) The EDS elemental mappings of MP@FS/BWO (all the scale bars are 500 nm). (g) XRD diagrams of paraffin, Fe_3O_4, MP@FS, and MP@FS/BWO.

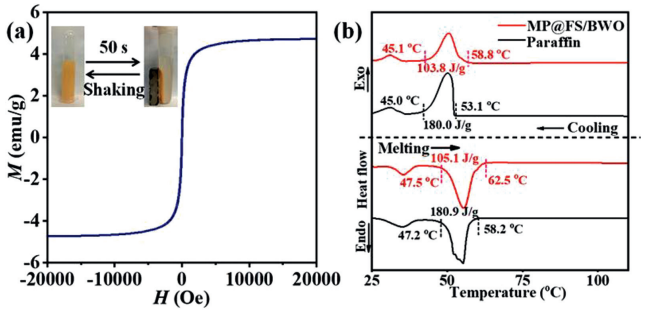

Fig. 2. (a) Magnetic hysteresis loop of MP@FS/BWO (The inset is the digital photographs of magnetic separation-redispersion process of MP@FS/BWO in aqueous suspension). (b) DSC curves of pure paraffin and MP@FS/BWO.

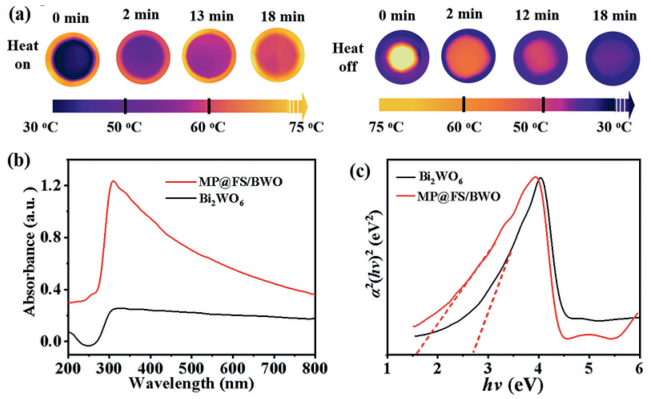

Fig. 3. (a) The real-time infrared thermographic images of MP@FS/BWO (located in the central part) taken after it is placed on a hot stage (75 °C). (b) UV–vis absorption spectra of MP@FS/BWO and Bi_2WO_6. (c) The corresponding plots of $(\alpha h\nu)^2$ - $h\nu$ of MP@FS/BWO and Bi_2WO_6 derived from (b).

of MP@FS/BWO can be calculated to be 57.1% according to the TG curve of MP@FS/BWO in Fig. 1c, and the residual mass is the total mass of Fe_3O_4 NP, SiO_2 shell and the loaded Bi_2WO_6. The mass fraction of Bi_2WO_6 in MP@FS/BWO can be calculated to be 8.6% by Eqs. S2 and S3 (see Fig. S3 part in Supporting information).

MP@FS/BWO has a type II N_2 adsorption-desorption isotherms (Fig. S2b in Supporting information), which is generally produced by non-porous or macroporous solids, indicating that the Bi_2WO_6 nanosheets fill the pores in the mesoporous silica shell. The BET specific surface area of MP@FS/BWO is reduced to 9.5 m^2/g.

The magnetic hysteresis loop of MP@FS/BWO can be seen in Fig. 2a, from which the saturation magnetization of MP@FS/BWO is determined to be 4.73 emu/g. The extremely low magnetic retentivity and coercivity of MP@FS/BWO allow them to be quickly separated from the medium completely in 50 s under a magnetic field. When the magnetic field is removed, the microcapsules can be evenly dispersed in the medium again by gently shaking, as shown in the inset in Fig. 2a.

The phase change behavior of MP@FS/BWO was investigated by differential scanning calorimetry (DSC), as shown in Fig. 2b, compared with that of uncoated paraffin. In order to remove the influence of thermal history on crystallization and melting, the samples were heated to 120 °C and kept for 1 min, then the crystallization and the following melting curves were recorded. It can be seen that the crystallization and melting behavior of MP@FS/BWO are very similar to those of pure paraffin. The phase change temperature range of MP@FS/BWO can be determined to be 47.5–62.2 °C by the crystallization and melting processes. The crystallization enthalpy of MP@FS/BWO is very close to the melting enthalpy. All the results indicated that MP@FS/BWO has the same phase change heat storage function as the paraffin wrapped in it.

Fig. 3a shows the real-time temperature change of MP@FS/BWO after it was placed on a hot stage of 75 °C. It can be seen that the temperature of MP@FS/BWO quickly rises from 30 °C to 50 °C after 2 min, but slowly increases from 50 °C to 60 °C in 9 min, and then rapidly increases to 75 °C in 5 min. When the heating of the hot stage is stopped, the temperature of MP@FS/BWO decreases as a similar trend to the heating process. The results indicate that MP@FS/BWO has a certain temperature regulation capability at a range of about 50–60 °C.

For visible light catalyst, the energy gap (E_g) is a critical parameter affecting its light absorption ability. The UV–vis absorption spectrum of MP@FS/BWO is measured to calculate the E_g of MP@FS/BWO, as shown in Figs. 3b and c. As a control, the UV–vis absorption spectrum of the micron-sized Bi_2WO_6 particles (~1.5 μm, Fig. S4 in Supporting information) prepared under the same hydrothermal reaction condition in the absence of MP@FS carrier is also exhibited. It is clearly seen that MP@FS/BWO has a strong absorption capacity for visible light with a wavelength up to 800 nm, while pure Bi_2WO_6 has a much weaker absorption in this wavelength range. The E_g of the sample can be calculated by the Tauc Eq. 1 according to the UV–vis absorption spectrum [34–37]:

$$(\alpha h\nu)^{1/n} = B(h\nu - E_g) \quad (1)$$

where α is the absorption coefficient, which can be calculated according to Beer-Lambert Law, $A = \alpha bc$, in which A is the absorbance, b is the thickness of the composite film (see Part I in Supporting information), and c is the concentration of the sample. h and ν are Planck's constant and light frequency, respectively. The value of n depends on the type of semiconductor. For Bi_2WO_6, it is a semiconductor with direct E_g, so n is 0.5. By extending the straight line portion of the plot of $(\alpha h\nu)^2$ - $h\nu$ (Fig. 3c) to the X-axis, the intersection value should be E_g, and B is a constant at this time. MP@FS/BWO has a much smaller E_g (1.60 eV) than Bi_2WO_6 (2.81 eV), indicating its excellent visible light absorption capacity. This should be related to the contribution of the deep color of MP@FS/BWO, as it has been reported that the dope with transitional ions including Fe^{3+} is an effective method to enhance the visible-light photocatalytic activity of catalysts [38].

The photocatalytic decomposition kinetics of rhodamine B (RhB) in the aqueous solutions containing MP@FS/BWO and Bi_2WO_6 of the same mass at room temperature under the irradiation of simulated sunlight are displayed in Fig. 4a and Fig. S5 (Supporting information). The decomposition of RhB catalyzed by MP@FS/BWO is very fast in the first 30 min, then slows down until it is completed at 120 min. However, in the same period of time, the decomposition rate of RhB in the Bi_2WO_6 system is much slower, 8% of RhB remains undecomposed. The decomposition of RhB is attributed to the N-demethylation and/or the destruction of the conjugated structure of RhB under the action of H^+,$^{\bullet}O^{2-}$ and $^{\bullet}OH$ radicals [8].

The MP@FS/BWO particles can be easily recovered from RhB catalytic decomposition system by magnetic separation. The catalytic performance of the recycled MP@FS/BWO is shown in Fig. 4b. It is seen that the decomposition ratio of RhB (D_{RhB}) remains above 99%, hardly changed after four cycles. The TEM image, XRD spectrum, and magnetic hysteresis loop of MP@FS/BWO after recycling were shown in Fig. S6 (Supporting information). Compared with Figs. 1e, 1g, and 2a, it can be seen that the morphology, crystal structure, and saturation magnetization of MP@FS/BWO are nearly unchanged after the photocatalytic reaction, indicating that MP@FS/BWO has an excellent structure stability and reusability.

In order to study the effect of phase change heat storage function on catalytic performance, the system was first placed in a wa-

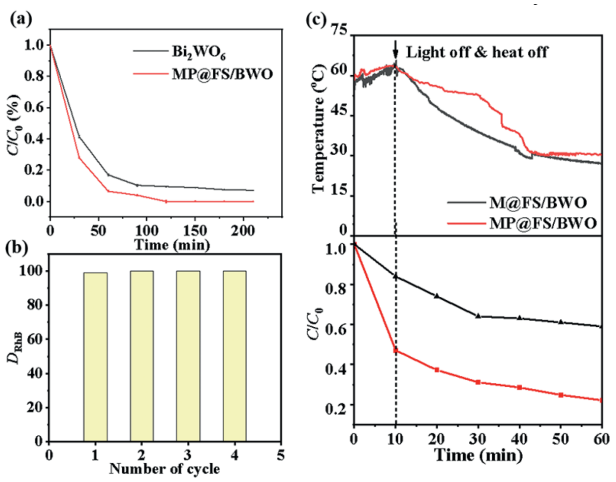

Fig. 4. (a) The decomposition kinetics of the RhB under the irradiation of simulated sunlight at room temperature. (b) The D_{RhB} measured when MP@FS/BWO was recycled for different times. (c) The temperature change and the decomposition kinetics of RhB when the systems were first placed in a water bath of 65 °C and irradiated with a xenon lamp for 30 min, then the system was transferred in a dark place at room temperature.

ter bath of 65 °C (above the phase change temperature of paraffin) and irradiated with a xenon lamp for 10 min. Then, the system was transferred in a dark place at room temperature for a certain time. The temperature change and the decomposition kinetics of RhB during the above process were recorded in Fig. 4c, as well as Figs. S5d and e. At the same time, another sample is prepared by removing paraffin core of MP@FS/BWO) using the calcination method (see Part I in Supporting information), and labeled as M@FS/BWO for comparison. It can be found that the degradation rates of RhB in these two systems are very fast under high temperature and light irradiation. The temperature of the MP@FS/BWO system drops slower than the M@FS/BWO system after the systems are taken away from the heating and lighting environment. In the same time, the decomposition rate of the MP@FS/BWO system is 78%, while it is 40.8% in the M@FS/BWO system. The results confirm that when the ambient temperature suddenly drops below the phase change temperature of paraffin, the MP@FS/BWO can maintain a high catalytic capacity to a certain extent by virtue of the self-temperature regulation function of phase change microcapsule carrier.

In Summary, novel submicron-sized magnetic phase-change-microcapsule-supported Bi_2WO_6 catalyst (MP@FS/BWO) are prepared successfully. MP@FS/BWO has a phase change enthalpy of 105.1 J/g in a temperature range of 50–60 °C, which endows the MP@FS/BWO with a certain self-temperature regulation ability. MP@FS/BWO shows excellent catalytic performance in the decomposition of RhB under the simulated sunlight irradiation. When the ambient temperature suddenly drops below the phase change temperature of paraffin, the MP@FS/BWO can maintain a high catalytic capacity to a certain extent by virtue of the self-temperature regulation function of phase change microcapsule carrier. The MP@FS/BWO can be easily recycled by magnetic separation and shows good structural stability and reusability. This work provides a way to prepare green, efficient multifunctional photocatalyst, which offers a new idea for the development of the future photocatalyst with long effect and energy saving for outdoor use.

Declaration of competing interest

The authors declare that they have no known competing financial interests or personal relationships that could have appeared to influence the work reported in this paper.

Acknowledgments

This work was supported by the National Natural Science Foundation of China (Nos. 51973205 and 51773189), and the Fundamental Research Funds for the Central Universities (Nos. WK9110000066, WK3450000005 and WK3450000006). The authors gratefully acknowledge Assoc. Prof. Huarong Liu in the Department of Polymer Science and Engineering of USTC for kindly providing the xenon lamp.

Supplementary materials

Supplementary material associated with this article can be found, in the online version, at doi:10.1016/j.cclet.2023.108637.

References

[1] G. Huang, S. Li, L. Liu, L. Zhu, Q. Wang, Appl. Surf. Sci. 503 (2020) 144183.
[2] F. Amano, A. Yamakata, K. Nogami, M. Osawa, B. Ohtani, J. Am. Chem. Soc. 130 (2008) 17650–17651.
[3] Q. Zhang, Z.W. Jiang, M.Z. Wang, X.W. Ge, Chin. J. Chem. Phys. 315 (2018) 701–706.
[4] N. Zhang, R. Ciriminna, M. Pagliaro, Y.J. Xu, Chem. Soc. Rev. 43 (2014) 5276–5287.
[5] H.D. Nie, K.Q. Wei, Y. Li, Chin. Chem. Lett. 32 (2021) 2283–2286.
[6] H.J. Dong, N. Song, M. Yan, Chin. Chem. Lett. 32 (2021) 2047–2051.
[7] M.J. Chen, Y. Huang, W. Chu, Chin. J. Catal. 40 (2019) 673–680.
[8] H.B. Fu, C.S. Pan, W.Q. Yao, Y.F. Zhu, J. Phys. Chem. B 109 (2005) 22432–22439.
[9] H. Yi, L. Qin, D. Huang, et al., Chem. Eng. J. 358 (2019) 480–496.
[10] Q. Zhang, J.X. Chen, Y.Y. Xie, M.Z. Wang, X.W. Ge, Appl. Surf. Sci. 368 (2016) 332–340.
[11] Z.W. Ni, Y. Shen, L.H. Xu, et al., Appl. Surf. Sci. 576 (2022) 151868.
[12] T.W. Chang, H. Ko, W.S. Huang, et al., Chem. Eng. J. 428 (2022) 131237.
[13] Z.N. Jiang, J.J. Shu, Z.Q. Ge, et al., Sol. Energy Mater. Sol. Cells 240 (2022) 111716.
[14] C.Y. Yuan, X.Q. Wang, X.Y. Yang, et al., Chin. Chem. Lett. 32 (2021) 2079–2085.
[15] Q. Zhang, Y.H. Wu, M.Z. Wang, et al., Mater. Res. Bull. 113 (2019) 223–230.
[16] Y.Z. Li, J.C. Huang, T. Peng, J. Xu, X.J. Zhao, ChemCatChem 2 (2010) 1082–1087.
[17] S. Kaneco, N. Li, K.K. Itoh, et al., Chem. Eng. J. 148 (2009) 50–56.
[18] J.C. Garcia, K. Takashima, J. Photochem. Photobiol. A: Chem. 155 (2003) 215–222.
[19] R.R. Ishiki, H.M. Ishiki, K. Takashima, Chemosphere 58 (2005) 1461–1469.
[20] H.Z. Zhang, X.D. Wang, D.Z. Wu, J. Colloid Interface Sci. 343 (2010) 246–255.
[21] X. Jiang, R.L. Luo, F.F. Peng, et al., Appl. Energy 137 (2015) 731–737.
[22] H.M. Yan, H.N. Yang, J.P. Luo, et al., Chin. Chem. Lett. 32 (2021) 3825–3832.
[23] Z.N. Jiang, W.B. Yang, F.F. He, et al., ACS Sustain. Chem. Eng. 6 (2018) 5182–5191.
[24] H. Liu, X.D. Wang, D.Z. Wu, Appl. Therm. Eng. 134 (2018) 603–614.
[25] F.X. Gao, X.D. Wang, D.Z. Wu, Sol. Energy Mater. Sol. Cells 168 (2017) 146–164.
[26] F.N. Li, X.D. Wang, D.Z. Wu, Energy Conv. Manag. 106 (2015) 873–885.
[27] L.X. Chai, X.D. Wang, D.Z. Wu, Appl. Energy 138 (2015) 661–674.
[28] Y. Zhang, X.Y. Li, J.Q. Li, et al., Nano Energy 53 (2018) 579–586.
[29] M. Jiang, J.J. Shu, H.Q. Jin, et al., J. Radiat. Res. Radiat. Process. 37 (2019) 050203.
[30] W.X. Yang, G.Q. Xu, J.J. Shu, M.Z. Wang, X.W. Ge, Chin. Chem. Lett. 32 (2021) 866–869.
[31] Y.Y. Xie, W.X. Yang, M.Z. Wang, X.W. Ge, Chem. Eng. J. 323 (2017) 224–232.
[32] J.X. Chen, S. Lei, K. Zeng, et al., Nano Res. 10 (2017) 2351–2363.
[33] Y.Y. Xie, J. Wang, M.Z. Wang, X.W. Ge, J. Hazard. Mater. 297 (2015) 66–73.
[34] J. Tauc, Optical Properties of Solids, in: F. Abeles (Ed.), Band Theory of Solids, North-Holland Publishing, Amsterdam, 1972, pp. 54–63.
[35] J.H. Noh, S.H. Im, J.H. Heo, T.N. Mandal, S.I. Seok, Nano Lett. 13 (2013) 1764–1769.
[36] G.S. Jamila, S. Sajjad, S.A.K. Leghari, M. Long, J. Hazard. Mater. 382 (2020) 121087.
[37] Y. Al-Hadeethi, M.I. Sayyed, Y.S. Rammah, Ceram. Int. 46 (2020) 2055–2062.
[38] M. Stefan, C. Leostean, O. Pana, et al., Appl. Surf. Sci. 390 (2016) 248–259.